DELFT UNIVERSITY OF TECHNOLOGY

REPORT 07-14

A mathematical approach to epidermal wound closure: Model Analysis and Computer Simulations

E. Javierre, F.J. Vermolen, C. Vuik and S. van der Zwaag

ISSN 1389-6520

Reports of the Department of Applied Mathematical Analysis

Delft 2007

A mathematical approach to epidermal wound closure: Model Analysis and Computer Simulations

E. Javierre, F.J. Vermolen, C. Vuik and S. van der Zwaag

Abstract

A computational algorithm to study the evolution of complex wound morphologies is developed based on a model of wound closure by cell mitosis and migration due to Adam [2]. A detailed analysis of the model provides estimated values for the incubation and healing times. Furthermore, a set of inequalities are defined which demarcate conditions of complete, partial and non-healing. Numerical results show a significant delay in the healing progress whenever diffusion of the epidermic growth factor responsible for cell mitosis is slower than cell migration. Results for general wound morphologies show that healing is always initiated at regions with high curvatures and that the evolution of the wound is very sensitive to the physiological parameters.

1 Introduction

Healing of cutaneous wounds proceeds by a combination of several interdependent chemical and mechanical processes. The healing process can be divided into three partly overlapping phases: the inflammatory, the proliferative and the remodelling phases [8]. The inflammatory phase starts immediately after injury and progresses during a few days. In this phase, bleeding and entry of infectious matter is stopped, the release of growth factors is triggered and phagocytes are attracted to clean the wound of contaminants. The proliferative phase extends in time up to a few weeks after injury and takes care of angiogenesis (repair of the vascular network), re-epithelialization (wound closure by mitosis and migration of epithelial cells into the wound), extracellular matrix synthesis (tissue that provides structural support to cells) and wound contraction (reduction of the wound area by tensile stresses). The remodelling phase lasts several months, and deals with the replacement of the extracellular matrix with scar tissue resembling, as much as possible, the parent (*i.e.* undamaged) tissue and the elimination of cells by apoptosis.

Mathematical modelling combined with computer simulations can help understanding the healing process and enlighten optimal conditions for treatments. Furthermore, models of healing mechanisms in nature are of inspiration in the development of materials with self-healing properties [19]. The monographs by Britton [4] and Murray [8] are good introductions to mathematical modelling of biological processes. Wound closure, by mitosis and migration of cells, has been studied by Adam *et al.* [2, 3, 17] and Sherrat *et al.* [15] among others. Angiogenesis has been modelled by Maggelakis [6, 7] and Gaffney *et al.* [5], and wound contraction by Murray [8] and Olsen *et al.* [9]. It is well known that these processes are inter-connected and influence one another during healing. However, as far as we know, they have never been coupled in a mathematical approach. It is our intention to develop a mathematical model that considers the three sub-processes and, by means of computer simulations, investigate their specific role in the healing process. Because of the complexity of this problem, in this work we focus on wound closure only. We present a simple model to track the wound evolution and give the foundations of our numerical method. In a subsequent work we will coupled this basic model with angiogenesis.

The present paper is organized as follows. First, the chemical model of wound closure, based on Adam's work [2, 3], is presented in Section 2 for general geometries. In this model, wound healing

is due to cell migration into the wound caused by a increased cellular and chemical activity in the surroundings of the wound. Subsequently, the computational method is described in detail in Section 3. A narrow band Level Set Method [1] is used to follow the wound edge. A standard Galerkin Finite Element Method, with adaptive local grid refinement around the wound edge, is implemented to compute the concentration of a generic epidermic growth factor that decides the locations of the wound edge that move towards healing. Afterwards, analytic solutions and conditions for complete healing are described for certain asymptotic cases in Section 4. Next, the influence of the physiological and geometrical parameters of the model on the healing kinetics is investigated in Section 5. Finally, the conclusions of our study are presented in Section 6. A full list of the parameters, physiological and numerical, used in our calculations is given in the Appendix.

2 The mathematical model for wound closure

In epidermal wounds, wound closure is entirely due to cell mitosis and migration. The mitotic activity is mainly responsible for the thickening of the epidermis, once the continuity of the basal membrane has been re-established. Since the thickness of the epidermis is very small compared to the wound dimensions, we will assume here that the wound is two dimensional. Hence, we will focus on the closure of the basal membrane by cell mitosis and migration, and disregard the thickening step.

In order to simplify the model, we consider a generic epidermic growth factor (EGF) that stimulates the increase of cellular activity in a layer surrounding the wound edge. The domain of computation Ω consists of the wounded region Ω_w, which is surrounded by the active layer Ω_{al} and the undamaged tissue Ω_u in the outer part, *i.e.* $\overline{\Omega} = \cup_i \overline{\Omega}_i$ and $\Omega_i \cap \Omega_j = \emptyset$ for $i, j \in \{w, al, u\}$ and $i \neq j$. The concentration c of the EGF within Ω is determined by the following reaction-diffusion equation

$$\frac{\partial c}{\partial t} - D\Delta c + \lambda c = P\chi_{\Omega_{al}(t)}, \tag{1}$$

which states the diffusional transport of the EGF through the epidermal tissue, its depletion or natural decay and its production. The characteristic function χ, which only has support in $\Omega_{al}(t)$, is used to account for the production of the EGF since it only takes place inside the active layer. The parameters D, λ and P respectively denote the diffusion, decay and production rates of the EGF. At the outer boundary of the domain Ω we impose a no-flux boundary condition, *i.e.* $\nabla c \cdot \mathbf{n} = 0$ where $\mathbf{n}$ denotes the normal vector.

Wound closure occurs by migration of cells inwards the wound. We define the wound edge Γ as the advancing front of cells. We assume that cells become motile if the accumulated EGF concentration exceeds a threshold value θ. Furthermore, cell migration may be interrupted if the EGF concentration drops below this threshold value. Therefore, in this approach cell motility is dose-dependent. Moreover, we assume that the rate at which the wound closes, *i.e.* the closure rate, is proportional to the local curvature of the wound edge [17]. Hence, the normal velocity v_n of the wound edge Γ is given by

$$v_n = \big(\alpha + \beta\kappa\big)H(c - \theta), \tag{2}$$

where $\alpha \geq 0$ and $\beta \geq 0$ (and $\alpha + \beta > 0$) denote the coefficients of the migration rate, κ denotes the local curvature of the wound edge and H represents the Heaviside function, defined as $H(x) = 0$ if $x < 0$ and $H(x) = 1$ if $x \geq 0$. Note that under this definition of the closure rate, the normal vector $\mathbf{n}$ points towards the wounded area.

Tracking the wound edge

The model, as presented here, falls within the category of moving boundary problems. The wound edge Γ, also referred to as the front position or interface, has to be determined at each time step

in order to identify the various parts of the domain of computation (wounded region, active layer and outer tissue) and to solve the concentration equation (1).

In this work, we use the Level Set Method [11] to follow the evolution of the wound edge in time. The wound edge is identified as the zero level set of a continuous function ϕ. At the initial time, we define the level set function ϕ as follows:

$$\phi(\mathbf{x},0) = \begin{cases} +\operatorname{dist}(\mathbf{x},\Gamma(0)), & \text{if } \mathbf{x} \in \Omega_w(0), \\ 0, & \text{if } \mathbf{x} \in \Gamma(0), \\ -\operatorname{dist}(\mathbf{x},\Gamma(0)), & \text{if } \mathbf{x} \in \Omega_u(0), \end{cases}$$

where we have arbitrarily chosen ϕ to be positive inside the wound, and negative outside. Using the total time-derivative of the level set function at the wound edge, we have that

$$0 = \frac{d}{dt}\phi\Big|_{\Gamma} = \frac{\partial \phi}{\partial t} + v_n ||\nabla \phi||. \tag{3}$$

This equation is only valid at the wound edge, but can be extended to the whole domain of computation if a velocity field $\mathbf{v}$ is determined satisfying the following conditions:

i) $\mathbf{v}(\cdot,t)$ is continuous over Ω, and

ii) its normal projection, $\mathbf{v}\cdot\mathbf{n}$, equals the closure rate v_n given in (2) at the wound edge.

We will present a simple velocity extension fulfilling constrains i) and ii) in the following section. For the time being, let us assume that such a velocity field $\mathbf{v}$ exists. The closure of the wound is then obtained by advection of the wound edge by means of the so-called level set equation:

$$\frac{\partial \phi}{\partial t} + \mathbf{v}\cdot\nabla\phi = 0. \tag{4}$$

Note that in this framework, the normal vector $\mathbf{n}$ and the curvature κ can be computed from ϕ as follows:

$$\mathbf{n} = \frac{\nabla\phi}{||\nabla\phi||}, \quad \kappa = \nabla\cdot\mathbf{n}.$$

The reader is referred to the books by Sethian [13] and Osher and Fedkiw [10] where a detailed presentation of the method and a wide collection of applications are given.

Re-initialization of ϕ

The level set function ϕ is initialized as a signed distance function. This choice enables us with an straightforward identification of the various subdomains in Ω. In particular, the wounded tissue corresponds to the region of ϕ being positive, and the active layer is given by

$$\Omega_{al}(t) = \{\ \mathbf{x}\in\Omega \mid 0 < -\phi(\mathbf{x},t) < \delta(\mathbf{x},t)\ \},$$

where δ denotes the local thickness of the active layer, which may depend on the local curvature of the wound edge [17]. To maintain the representation of the active layer accurate, the level set function should remain a signed distance function after advection (4), at least a distance δ from its zero level set. Normally, this property is lost if time increases, and several remedies have been suggested for its repair. The most extended methods for this problem solve the Eikonal equation

$$||\nabla\phi|| = 1, \tag{5}$$

either iteratively [12, 16] or directly [14, 18]. The iterative methods are very competitive if we wish to keep ϕ a distance function in a thin band, of a couple of grid nodes, around the interface. However, the computational cost increases as the bandwidth gets larger, and eventually, the direct methods are computationally cheaper. In our case, the bandwidth depends on the active layer thickness, which may be large compared to the grid size. Therefore, we will use a direct method, the Fast Marching Method [14], to solve (5).

3 The computational approach

The solution of equation (1) is approximated by using a Finite Element Method with piecewise linear basis functions. Further, we have to deal with a moving interface and with a sharp (discontinuous) change of the production of the EGF across the edges of the active layer. Tracking the wound edge position in time with the Level Set Method allows us to deal in a straightforward manner with wounds of a complicated geometry involving morphological changes. Supplementing the Finite Element Method with a local refinement of the elements neighbouring the wound edge results into a more accurate representation of the EGF concentration and into higher grid resolutions for the computation of the closure rate in an efficient way.

As a background or fixed basis mesh we use a structured triangulation with linear elements, see Figure 1 (left) and, at each time step, the elements close to the interface are refined, see Figure 1 (center), according to a criterion that is specified below. After refinement, the refined region presents a Cartesian structure, see Figure 1 (right), where the (nonlinear) hyperbolic equations inherited from the level set formulation can be easily solved with finite difference or finite volume schemes.

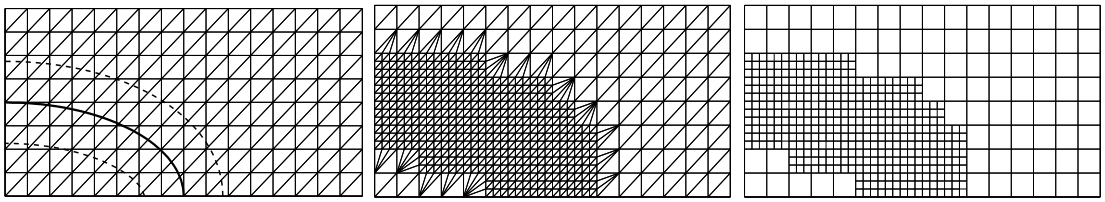

Figure 1: Left: fixed base FE mesh with the interface position $\phi = 0$ (solid curve) and the contours $\phi = \pm dist$ (dashed curves). The elements within these contours are to be refined. Center: refined FE mesh. Right: the nested Cartesian grids.

Hence, in order to compute the solution (*i.e.* EGF concentration and wound edge location) at a certain time step, we need to perform a number of steps. Globally speaking, first we have to compute the velocity field $\mathbf{v}$ from the EGF concentration profile at the previous time step. Next, the level set function has to be updated to obtain the wound edge location at the next time step. Subsequently, ϕ has to be reinitialized to a distance function in order to obtain an accurate representation of the active layer, and finally, the partial differential equation (1) is solved to find the EGF distribution at the next time step. However, since the fixed basis mesh is adapted to the wound edge each time step, there are a few communication steps that have to be taken carefully. The complete algorithm is presented in Algorithm 1.

Regularizations of the characteristic and heaviside functions

Cell motility is determined by interpolation of the EGF concentration at the wound edge. The discontinuous production term $P\chi$ is regularized in order to diminish numerical wiggles present at the edges of the active layer which may spoil the computation of the closure rate. Therefore, instead of the characteristic function χ we use a regularized version χ_ε defined as follows:

$$\chi_\varepsilon(\phi) = \begin{cases} \frac{1}{2}\Big[1 + \sin\left(\frac{\pi}{\varepsilon}(\phi + \frac{\varepsilon}{2})\right)\Big], & \text{if } 0 < \phi < \varepsilon, \\ 1, & \text{if } 0 \le \phi \le -\delta, \\ \frac{1}{2}\Big[1 + \sin\left(\frac{\pi}{\varepsilon}(\phi + \delta + \frac{\varepsilon}{2})\right)\Big], & \text{if } -\delta < \phi < -\delta - \varepsilon, \\ 0, & \text{otherwise,} \end{cases}$$

where ε is a parameter defined by the user to establish across how many grid cells the regularization is applied. In our numerical computations we use $\varepsilon = 1.5 \cdot \max(\Delta x_{Ref}, \Delta y_{Ref})$, where Δx_{Ref} and

Algorithm 1 Computation of the solution at time $t + \Delta t$ from the the solution at time t

Input: c, ϕ and refined finite element mesh at time t
Output: v_n, Δt, c, ϕ and refined finite element mesh at time $t + \Delta t$

1: Extend v_n over the refined Cartesian band, compute $\mathbf{v} = v_n \mathbf{n}$
2: Choose time step Δt according to $\mathbf{v}$
3: Solve level set equation (4) over the refined Cartesian band
4: Re-initialize ϕ inside the refined Cartesian band
5: Map ϕ to the global coarse Cartesian grid (note that ϕ is not yet defined over the nodes outside the refined Cartesian band)
6: Extend ϕ outside the (coarse) Cartesian band solving $||\nabla \phi|| = 1$
7: Compute the refined finite element grid according to the new position of the interface
8: Map concentration profile on the previous refined FE triangulation to the current refined FE triangulation
9: Map ϕ from the nested Cartesian grids to the refined FE triangulation
10: Compute the production term over the refined FE triangulation
11: Solve concentration equation (1) over the refined FE triangulation
12: Map concentration at the refined FE triangulation to the refined Cartesian grid

Δy_{Ref} denote respectively the grid size of the refined band in the x and y directions. A similar regularization could be adopted for the definition of the closure rate, though the standard definition of the heaviside function has been used in our calculations.

3.1 The local grid refinement strategy

Due to the structure of the fixed basis mesh, its refinement in the vicinity of the front position is straightforward if the level of refinement (LOR) is known element-wise.

We say that an element e is within a distance $dist$ from the interface if one or more of its vertices e_i is within a distance $dist$ from the interface (*i.e.* $|\phi(e_i)| < dist$ for $i \in \{1, 2, 3\}$). All elements within a distance $dist$ from the interface are labeled with the maximum LOR, that is 2. If $dist$=0, elements intersected by the interface are marked with the maximum LOR. Elements adjacent to those with maximal LOR are labeled, in principle, with a lower LOR, that is 1. However, to preserve mesh consistency, their LOR has to be increased when they are adjacent to more than one element with maximum LOR. This step is illustrated in Figure 2. Elements further away are labeled with zero LOR, meaning that they are not refined.

The division of the elements, according to their LOR, is based on the division of the edges. Let us denote by $refnratio$ the number of equally sized sub-edges that appear when the edge of an element is refined. If the LOR of an element is 2, then all the edges are divided into $refnratio$ sub-edges, and the element is divided into $refnratio^2$ sub-elements. If the LOR is 1, only the edge in common with the neighbouring element with LOR equal to 2 is refined. Consequently, the element is divided into $refnratio$ sub-elements, see Figure 2.

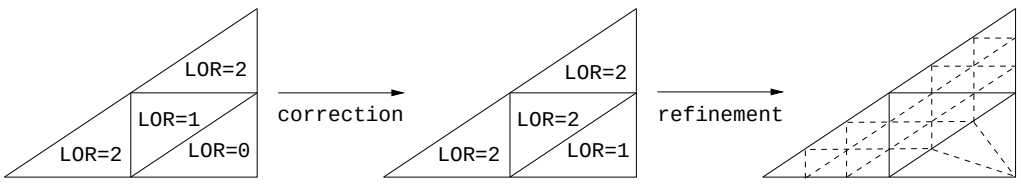

Figure 2: Correction of the LOR and subsequent subdivision of the elements, with $refnratio$=3.

In order to prevent excessively narrow elements, which may impair the accuracy of the results, we will restrict ourselves to ratios of refinement, $refnratio$, of 2 or 3. To balance the additional work invested in the refinement with the gain in accuracy and CPU-times, we define $dist$ such that the elements intersected by the interface and the elements adjacent to them receive the maximum LOR. Hence, $dist \gtrsim \sqrt{\Delta x^2 + \Delta y^2}$, where Δx and Δy denote the element size of the basis mesh. Furthermore, we shall impose a maximum displacement bound on the time stepping to prevent that the level of refinement of the elements close to interface changes by more than one within two consecutive time steps. As we will see below, this is ensured by a CFL condition on the advection of the level set function.

The transition between two consecutive refined grids (*i.e.* two consecutive time steps) can be implemented efficiently if the LOR of the previous mesh is stored in memory. By construction, the LOR of an element at the new time step either does not change, or increases by one, or reduces by one its LOR at the previous time step. If the LOR does not change, the refinement of the element is the same as in the previous time step. If the LOR is reduced by one, the element is coarsen. Finally, if the LOR is raised by one, then the refinement of the element increases.

3.2 The two nested Cartesian grids

Due to its structure, the nodes of the background triangulation form will be referred to as the coarse Cartesian grid. Moreover, after refinement, the refined region resembles a refined Cartesian band which is nested in the coarse Cartesian grid, see Figure 1 (left). We use both grids to solve the hyperbolic equations inherited from the level set formulation.

3.2.1 The narrow band level set method

In order to update the front position we first need to compute an extension of the front velocity, and subsequently solve the level set equation (4). This operations are carried out within the refined Cartesian band.

Extension of the front velocity off the interface

The front velocity v_n is only defined at the interface location, and an artificial extension of it is required to solve the level set equation (4). As stated before, this extension should be such that the extended velocity field is continuous. To achieve this, we advect the front velocity outwards in the proper upwind direction, by solving

$$\frac{\partial v_n}{\partial \tau} + \mathrm{S}(\phi)\mathbf{n} \cdot \nabla v_n = 0, \tag{6}$$

where τ denotes a fictitious time used only in the extension procedure and $\mathbf{n}$ denotes the normal vector, which points towards increasing values of ϕ (*i.e.* in the direction of the gradient of ϕ, and note that $\phi > 0$ inside the wound). Thus, with this equation, information is transported from the wound edge inside the wound (when $\phi > 0$) and outside the wound (when $\phi < 0$). Note that at the wound edge, the previous equation is degenerated, since $\mathrm{S}(\phi) = 0$, and hence the value of v_n is not altered there.

The solution of (6) is computed only inside the refined Cartesian band, as described in Algorithm 2. We perform a small number of pseudo-time iterations $IterMax$, between 5 and 10, since it is enough to obtain a continuous extension of v_n in the band around the interface. The normal vector $\mathbf{n} = \nabla\phi/||\nabla\phi||$ is approximated with central differences inside the band and first order sided differences at the boundary. The local curvature $\kappa = \nabla \cdot \mathbf{n}$ is computed analogously.

Interface advection and re-initialization of ϕ to a distance function

Algorithm 2 Extension of the front velocity onto the refined Cartesian band

Initialization of v_n

1: Initialize v_n=0 inside the band
2: **if** $\mathbf{x}$ is a node adjacent to the interface **then**
3: Compute associated interface point $\mathbf{x}_f = \mathbf{x} - \phi(\mathbf{x})\mathbf{n}$ (linear interpolation of ϕ)
4: Compute $v_n(\mathbf{x}_f)$ according to (2) (use bicubic interpolation of c and κ)
5: Assign $v_n(\mathbf{x}_f)$ to $\mathbf{x}$
6: **end if**

Advection of v_n off the interface position

1: **for** $Iter = 1$ to $IterMax$ **do**
2: Solve (6) for the points not being adjacent to the interface
Time integration: Forward Euler; spatial derivatives: first order upwind discretizations
3: **end for**

Set $\mathbf{v} = v_n\mathbf{n}$

After the advection field $\mathbf{v} = (u, v)^t$ is defined over the band, the level set equation (4) is solved inside the band. The time integration is carried out with the Euler forward method, whereas the space derivatives are discretized with a first order accurate upwind scheme. The CFL stability condition is satisfied if the time step Δt is chosen such that

$$\Delta t \leq \Delta t_{CFL} := \frac{CFL}{\max\left(\frac{u}{\Delta x} + \frac{v}{\Delta y}\right)}, \quad CFL < 1. \tag{7}$$

In practice, we will take $\Delta t = \min(\Delta t_{CFL}, \Delta t_{max})$, where Δt_{max} is used as a default time step during the incubation periods and prevents the use of excessively large time steps when the front velocity is close to zero. With this choice of Δt, the wound edge will travel over a distance smaller than the grid size during each time step, which is consistent with the grid refinement algorithm.

Despite that the level set function ϕ is initialized as a distance function, the function $\tilde{\phi}$ resulting from the advection of the interface is no longer a distance function. Generally, its deviation after one time step is small, and re-initialization may be evitable. However, the error accumulates, and after several time steps re-initialization is unavoidable. In our case, we use a second order accurate Fast Marching Method to solve the Eikonal equation $||\nabla\phi|| = 1$ inside the band. This method proceeds as follows. First, the function ϕ is initialized at the nodes adjacent to the interface in such a way that the zero level set of $\tilde{\phi}$ is not altered. Subsequently, ϕ is extended away in the downwind direction. Details of this method can be found in the work by Sethian [14].

3.2.2 Extension of ϕ outside the band

In order to extend ϕ further away, *i.e.* outside the refined Cartesian band, we first map it to the coarse Cartesian band (*i.e.* to the nodes which lay both in the refined band and in the coarse global grid) and subsequently we extend ϕ outside the band with the Fast Marching Method. As a result, we obtain a function ϕ that is defined on the basis mesh, which does not alter the interface position, and which is a distance function.

4 Asymptotic solutions

This section is devoted to study two simplified problems. In the first case, we consider the healing process in absence of transport of the EGF, which prevents the supply of EGF to the wound site. In the second case, we look at the healing process with instantaneous diffusion of the EGF, which provides the wound with a suboptimal EGF distribution. By analysis of their analytic solutions,

we will give valuable insights to the healing behaviour predicted by the model and start to discern the role of some parameters in the model.

We define t_{inc} as the incubation time that is necessary to activate the closure of the wound. Hence, t_{inc} is the smallest positive time at which $c(\mathbf{x}, t_{inc}) \geq \theta$ for any point $\mathbf{x}$ on the initial wound edge. After this time, the healing process starts and the wound size decreases. However, new storage or incubation periods may become necessary as healing progresses if the EGF level at the wound edge falls below θ. Hence, we can describe the healing process as a series of healing and incubation periods as sketched in Figure 3, where $\mathcal{I}^i_{heal}$ $(i = 1, 2, \dots)$ denotes the healing period within the consecutive incubation periods $\mathcal{I}^{i-1}_{inc}$ and $\mathcal{I}^i_{inc}$. By convention we denote by t^i_{inc} and t^i_{heal} the times at which $\mathcal{I}^i_{inc}$ and $\mathcal{I}^i_{heal}$ finish respectively, which are formally defined as

$$t^i_{heal} := \min\big(t > t^{i-1}_{inc} \mid c(\mathbf{x}, t) < \theta \ \text{ for all } \ \mathbf{x} \in \Gamma(t)\big), \ i \geq 1,$$
$$t^i_{inc} := \min\big(t > t^i_{heal} \mid c(\mathbf{x}, t) \geq \theta \ \text{ for any } \ \mathbf{x} \in \Gamma(t^i_{heal})\big), \ i \geq 1.$$

We extend this convention by denoting $\mathcal{I}^0_{inc}$ the first or initial incubation period, $t^0_{inc} = t_{inc}$ and t^0_{heal}=0. For sake of the presentation, we will refer to $\mathcal{I}^i_{inc}$ for $i \geq 1$ as internal incubation periods.

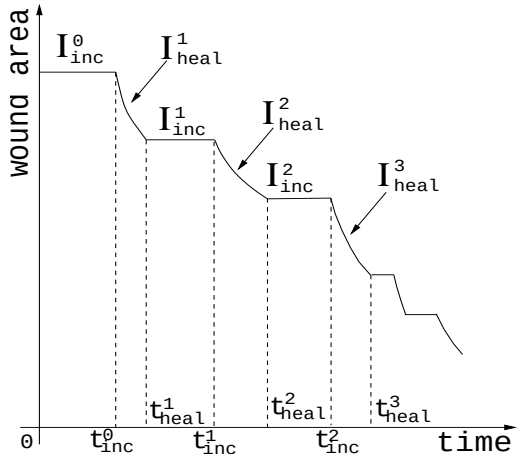

Figure 3: Schematic diagram of the healing process

4.1 No diffusional transport of the EGF

If we assume that there is no diffusional transport of the EGF from the active layer towards the wound, *i.e.* D=0, then the whole production of EGF is maintained inside the active layer and no EGF flows into the wound. Hence, during a whole incubation period $\mathcal{I}^i_{inc}$, the EGF concentration is given by

$$\frac{\partial c}{\partial t} + \lambda c = P\chi_{\Omega_{al}(t^i_{heal})},$$

with initial condition the concentration at the beginning of the incubation period, *i.e.* $c(\mathbf{x}, t^i_{heal})$. Integration in time of the above equation yields:

$$c(\mathbf{x}, t) = \exp\big(-\lambda(t - t^i_{heal})\big)c(\mathbf{x}, t^i_{heal}) + \frac{P}{\lambda}\chi_{\Omega_{al}(t^i_{heal})}(\mathbf{x})\Big(1 - \exp\big(-\lambda(t - t^i_{heal})\big)\Big),$$

for $\mathbf{x} \in \Omega$ and $t \in \mathcal{I}^i_{inc}$. Moreover, since the EGF production is not diffused towards the wound from the active layer, the concentration at the wound edge decays to zero as soon as it moves and

hence $c(\mathbf{x}, t^i_{heal}) = 0$ for all $\mathbf{x} \in \Gamma(t^i_{heal})$. Therefore, the concentration at the wound edge is given by

$$c(\mathbf{x}, t) = \frac{P}{\lambda}\Big(1 - \exp\big(-\lambda(t - t^i_{heal})\big)\Big), \quad \text{for } \mathbf{x} \in \Gamma(t^i_{heal}),\ t \in \mathcal{I}^i_{inc},$$

and the healing process will be initiated or resumed within a finite time if and only if

$$\lim_{t\to\infty} \frac{P}{\lambda}\Big(1 - \exp\big(-\lambda(t - t^i_{heal})\big)\Big) > \theta, \tag{8}$$

i.e. if and only if $P/\lambda > \theta$. This condition was also found by Adam in [2] using the analytic solution of the steady-state problem, and manifests the necessity for the production inside the active layer to overcome the depletion as the concentration reaches the threshold level θ. It is worth noting that, in the case of no diffusion of the EGF, the thickness or shape of the active layer does not play any role.

Finally, if the healing process can be sustained, *i.e.* $P/\lambda > \theta$, then the initial incubation time t_{inc} is given by

$$t^{D=0}_{inc} = \frac{1}{\lambda}\log\left(\frac{1}{1 - \frac{\lambda\theta}{P}}\right). \tag{9}$$

Furthermore, as the closure of the wound is permanently interrupted to restore the EGF concentration at the wound edge, healing of the wound will just not occur. The EGF concentration at the edge of a circular wound during the first three incubation periods is plotted in Figure 4, where the "broken" healing behaviour of the solution can be observed.

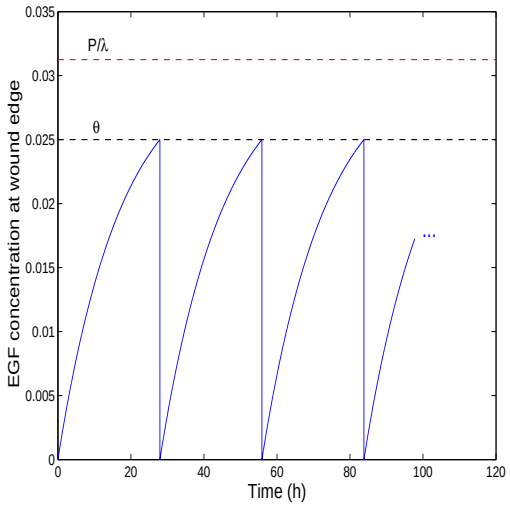

Figure 4: Time progression of the EGF concentration at the edge of a circular wound for the case of D=0. The horizontal line indicates the upper bound for the threshold value θ in order to initiate healing.

4.2 Instantaneous transport of the EGF

In the case of an instantaneous diffusion of the EGF, the production inside the active layer is immediately distributed throughout the whole domain of computation and the EGF concentration shows a flat profile over time. Hence, by integration of equation (1) over Ω, we can define an effective production rate

$$P_{eff}(t) := P\frac{|\Omega_{al}(t)|}{|\Omega|},$$

where $|\mathcal{A}|$ denotes the area of $\mathcal{A}$. With this definition, the EGF concentration is given by the solution of

$$\frac{dc}{dt} + \lambda c = P_{eff}(t), \tag{10}$$

with initial condition $c(0) = 0$. The definition of P_{eff} indicates the relevance of the area of the active layer in the healing process. For instance, if the thickness of the active layer is kept constant during healing, then the area of Ω_{al} decreases and hence the production sustained by it diminishes as the wound heals. Despite that this seems adequate since the wound area decreases, it may result into an incomplete healing of the wound as we will show below.

The exact integration of (10) is not always possible since P_{eff} depends on the evolution of the wound. However, it can be solved during the incubation periods, since then P_{eff} is constant. Hence, the EGF concentration during the ith incubation period $\mathcal{I}^i_{inc}$ is given by

$$c(t) = \frac{P_{eff}(0)}{\lambda}\Big(1 - \exp\big(-\lambda t\big)\Big), \quad \text{for } i = 0,$$
$$c(t) = \exp\big(-\lambda(t - t^i_{heal})\big)\theta + \frac{P_{eff}(t^i_{heal})}{\lambda}\Big(1 - \exp\big(-\lambda(t - t^i_{heal})\big)\Big), \quad \text{for } i \geq 1.$$

Because of the continuity of c, it is easy to see that the healing process will be initiated or continued if and only if

$$\frac{P_{eff}(t^i_{heal})}{\lambda} > \theta, \text{ for } i \geq 0, \iff \frac{P}{\lambda}\frac{|\Omega_{al}(t^i_{heal})|}{|\Omega|} > \theta, \text{ for } i \geq 0.$$

Hence, in the case of instantaneous transport of the EGF, the healing process will start if and only if

$$\frac{P}{\lambda} > \theta\frac{|\Omega|}{|\Omega_{al}(0)|}, \tag{11}$$

which, for fixed decay rate λ and threshold concentration θ, provides a lower bound for the production rate P as function of the active layer and the animal sizes. Thus, if the conditions for the initiation of the healing process hold, the initial incubation time is given by

$$t^{D\to\infty}_{inc} = \frac{1}{\lambda}\log\left(\frac{1}{1 - \frac{\lambda\theta}{P}\frac{|\Omega|}{|\Omega_{al}(0)|}}\right). \tag{12}$$

Note furthermore that initiation of the healing process is much more demanding in the case of fast diffusion processes, as can be seen by comparison of equations (8) and (11), since it is reasonable to expect that $|\Omega|/|\Omega_{al}(0)| \gg 1$. On the other hand, stoppage of wound closure after initiation is due to an insufficient EGF production, and hence $c'(t^i_{heal}) < 0$ at the stopping times t^i_{heal} $(i \geq 1)$. Therefore, once the healing process is stopped, it can never be resumed.

The analytic expression of the EGF concentration during healing can be obtained for certain definitions of the active layer and the mitotic rate. In the remaining of this section we consider the healing response of a circular wound of radius r_0 in a circular domain of computation of radius R_c and an active layer of constant thickness δ. In this case, the area of the active layer is given by

$$|\Omega_{al}(t)| = \pi\delta(2r(t) + \delta),$$

where $r(t)$ denotes the wound radius at time t. If in addition we take β=0, then

$$r(t) = r_0 - \alpha\big(t - t_{inc}\big),$$

and

$$c(t) = \theta\exp\big(-\lambda(t - t_{inc})\big) + \frac{P\delta}{R_c^2\lambda^2}\left\{\lambda\Big(2r(t) + \delta\Big) + 2\alpha - \exp\big(-\lambda(t - t_{inc})\big)\Big(\lambda(2r_0 + \delta) + 2\alpha\Big)\right\}, \tag{13}$$

during the first healing period, *i.e.* $t \in \mathcal{I}^1_{heal}$. The complete healing of the wound occurs if and only if there is a time $t_{heal} > t_{inc}$ such that $r(t_{heal})=0$ and $c(t_{hea}) > \theta$. It is easy to see, after simple algebraic manipulations, that this condition is equivalent to

$$\theta < \frac{P\delta}{R_c^2\lambda^2}\frac{2\alpha+\lambda\delta-\exp\big(-\frac{\lambda r_0}{\alpha}\big)\Big(2\alpha+\lambda(2r_0+\delta)\Big)}{1-\exp\big(-\frac{\lambda r_0}{\alpha}\big)},$$

which establishes the healing success as a function of the physiological parameters of the model. Table 1 summarizes the healing response for several values of θ and α.

θ	α	healing
$\leq \frac{P}{\lambda}\frac{\delta^2}{R_c^2}$	any	complete
$\in \Big(\frac{P}{\lambda}\frac{\delta^2}{R_c^2}, \frac{P}{\lambda}\frac{\delta(r_0+\delta)}{R_c^2}\Big]$	large small	complete incomplete
$\in \Big(\frac{P}{\lambda}\frac{\delta(r_0+\delta)}{R_c^2}, \frac{P}{\lambda}\frac{\delta(2r_0+\delta)}{R_c^2}\Big]$	any	incomplete
$> \frac{P}{\lambda}\frac{\delta(2r_0+\delta)}{R_c^2}$	any	not initiated

Table 1: Description of the healing response as function of the physiological parameters of the model.

For the cases in which the healing is not complete, the wound radius at the stopping time can be computed from equation (13), since then there is a time $t_{stop} > t_{inc}$ such that $c(t_{stop}) = \theta$ and $r_{stop} := r_0 - \alpha(t_{stop} - t_{inc})$, which yields

$$\theta = \frac{P\delta}{R_c^2\lambda^2}\frac{2\alpha+\lambda\big(2r_{stop}+\delta\big)-\exp\big(-\lambda\frac{r_0-r_{stop}}{\alpha}\big)\Big(2\alpha+\lambda\big(2r_0+\delta\big)\Big)}{1-\exp\big(-\lambda\frac{r_0-r_{stop}}{\alpha}\big)}.$$

The healing behaviour of a circular wound in the case of instantaneous diffusion of the EGF is shown in Figure 5. The EGF concentration during time is plotted in Figure 5(a) for two different values of θ, of which the smallest gives complete healing of the wound whereas the largest yields incomplete healing. The healing response and wound radius at stop for a wide range of closure rates is presented in Figure 5(b), where the reduction of r_{stop} towards successful healing (*i.e.* $r_{stop} = 0$) by the increase of the migration rate can be observed.

Healing time

If healing is complete (see Table 1), then it proceeds directly after incubation without internal incubation times. Hence, the wound evolution after initiation is the same as if the threshold condition upon cell motility is disregarded or θ is set equal to zero. Therefore,

$$t^{D\to\infty}_{heal} = t^{D\to\infty}_{inc} + t^{\theta=0}_{heal}.$$

Computation of $t^{\theta=0}_{heal}$ for general wound morphologies only requires the solution of (4) with $v_n = \alpha + \beta\kappa$, which is much easier than the solution of the complete problem. Furthermore, $t^{\theta=0}_{heal}$ is known for simple wound morphologies [17].

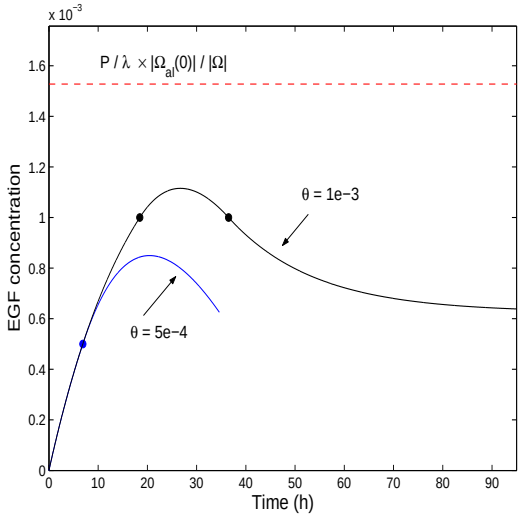

(a) Time evolution of the EGF concentration for two different values of θ. The horizontal line indicates the upper bound for θ in order to initiate healing.

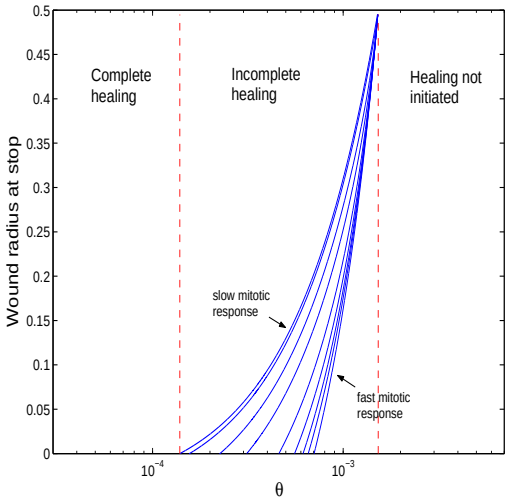

(b) The healing response in the case of $D \to \infty$ for several closure rates. Under this notation, successful healing is obtained when r_{stop}=0.

Figure 5: Healing of a circular wound with instantaneous diffusion of the EGF.

5 Analysis of healing kinetics

The specific role of diffusion and cell migration rates in the healing behaviour described by equations (1), (2) and (4) are discussed here. Results for a circular wound under various physiological conditions will show the strong interdependence between these processes and their impact on the healing kinetics.

5.1 The role of diffusion in the healing kinetics

The diffusion term in (1) is responsible for the supply of the necessary EGF to the wound in order to sustain its healing. We have seen in Section 4 that in absence of diffusion, the incubation time t_{inc} is minimal but healing is not obtained in a finite time. On the other hand, if diffusion is instantaneous, the incubation time is exponentially increased by the ratio of the domain of computation and the active layer areas, *i.e.* $|\Omega|/|\Omega_{al}(0)|$. Furthermore, in the case of successful healing, it proceeds directly after incubation.

The incubation and healing times for a wide range of diffusion rates D are plotted in Figure 6(a). The incubation time continuously increases as the diffusion rate increases, as the EGF is sent far from the interface delaying its accumulation. Furthermore, the results for the incubation times as $D \to 0$ and $D \to \infty$ agree perfectly with the asymptotic values given in (9) and (12) respectively. Besides that, we observe that the healing time increases exponentially as the diffusion rate decreases, since then the closure of the wound is faster than the EGF diffusion into the wound. This implies, numerically, more and longer internal incubation times, and physiologically the impossibility to sustain the healing process. As D increases, the healing time reduces until it reaches its minimum. This minimal healing time is obtained when the diffusion and the closure rates are balanced. We denote by D_{crit} the critical diffusion rate that gives the minimal healing time. We observe that the difference between the healing and the incubation times remains constant for diffusion rates above D_{crit}, and the time consumed between incubation and healing agrees with the healing time of the wound with θ=0. This means that if $D > D_{crit}$, then the healing progress is not delayed by internal incubation times and therefore the increase of the healing time is entirely due to the increase of the incubation time. Furthermore, in these cases the closure of the wound

is slower than the diffusion of the EGF into the wound.

As a consequence of the behaviour of the healing time with respect to the diffusion rate, there exist pairs of diffusion rates that result in the same healing time. The evolution of the wound radius for one of these pair is presented in Figure 6(b). As is to be expected, the healing at the lower diffusion rate is initiated earlier. However, for the higher diffusion rate, the evolution of the wound radius after initiation is the same as for θ=0, whereas it is delayed for the lower diffusion rate.

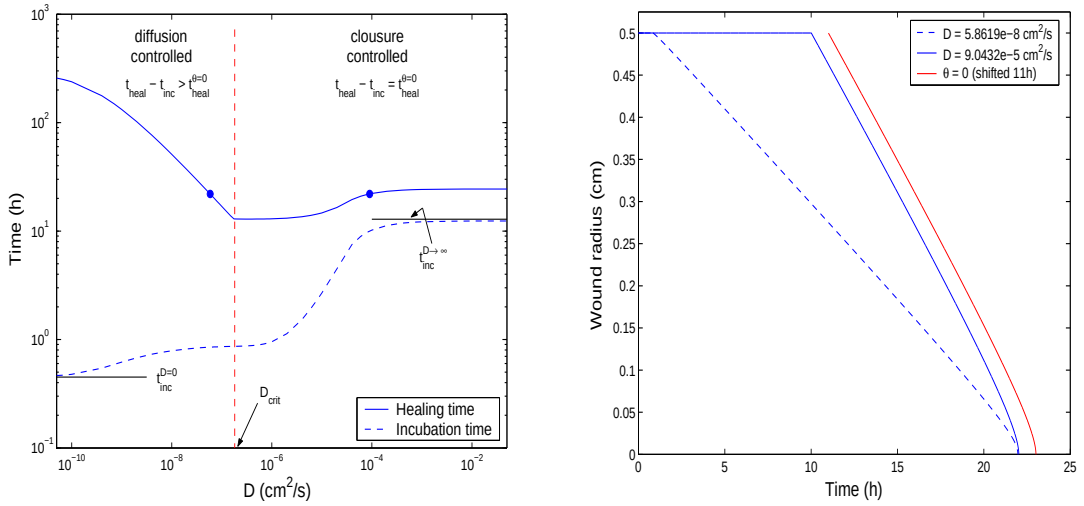

(a) Incubation and healing times as a function of D

(b) Healing behaviour for two different values of D that give the same healing time.

Figure 6: Influence of the diffusion term in the healing behaviour.

5.2 The role of the closure rate in the healing kinetics

In the previous section we have seen that the healing process is optimal, in the sense that it is not delayed, if the wound closure is slower than the diffusion of the EGF into the wound. In this section, we will measure the delay of the healing process due to the closure rate.

The delay in the healing process can be measured by

$$t_{delay} = \left(t_{heal} - t_{inc}\right) - t_{heal}^{\theta=0}, \tag{14}$$

which primarily depends on the threshold condition θ and on the migration rate parameters α and β. Furthermore, we can define a delay or retardation factor as follows:

$$f_{delay} := \frac{t_{heal}^{\theta=0}}{t_{heal} - t_{inc}}, \tag{15}$$

which equals 1 if there is no delay and is smaller than 1 if there is some delay. Hence, the healing kinetics for any threshold condition $\theta > 0$ can be expressed as a delay of the healing kinetics for θ=0, since $t_{heal} = t_{inc} + t_{heal}^{\theta=0}/f_{delay}$. The delay factor for a circular wound as a function of θ and α is presented in Figure 7 for two different diffusion rates. The contribution to the closure rate of the wound curvature β is disregarded in this test, *i.e.* β=0. The results show that for either low migration rates or θ values no delay is obtained. However, there is an exponential decrease of the delay factor as α and θ increase, since then the diffusion term is not capable of sustain the necessary flux of EGF into the wound. Furthermore, comparison of the results for the two

different diffusion rates evidences that larger diffusivities mitigates the delayed kinetics for a wider range of θ and α. This agrees with the results obtained in the previous section.

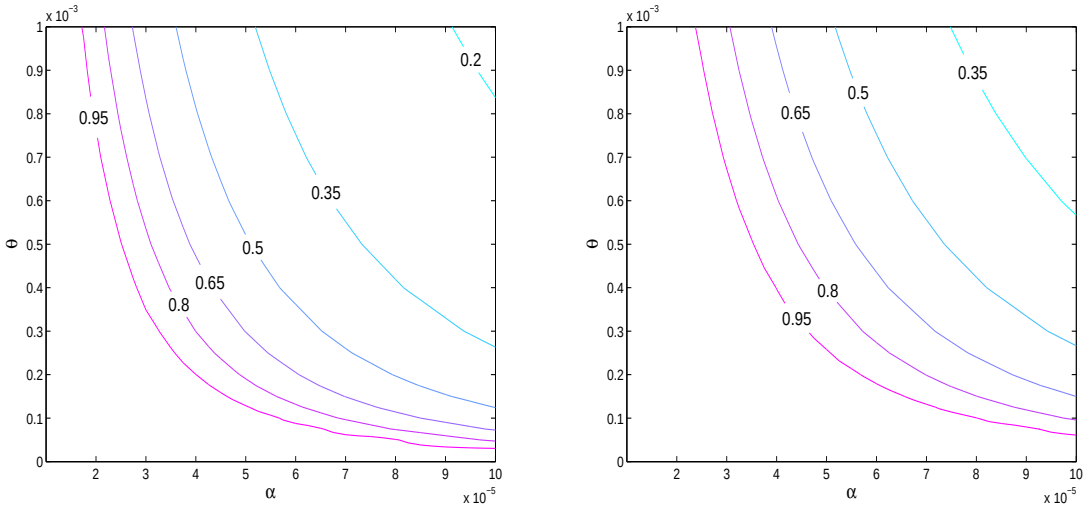

(a) D=5·10^{-7} cm^2/s (b) D=10^{-6} cm^2/s

Figure 7: Isocurves of the delay factor f_{delay} as a function of the closure rate α and the threshold concentration θ for two diffusion rates. The contribution of the curvature to the closure rate has been disregarded, *i.e.* β=0. Hence, the healing time for θ=0 is given by $t_{heal}^{\theta=0} = \frac{r_0}{\alpha}$.

5.3 The effect of wound geometry on healing kinetics

The role in the healing kinetics of wound morphology is investigated in this section. To this end, we start with the healing of an elliptical wound of area 0.78540 cm^2 with various elongations. In this simulation, we neglect the mechanical forces acting on the tissue. Due to the symmetry of the problem, we solve only one quarter of the ellipse. The incubation times for various wound elongations and θ values are presented in Figure 8(a). As can be seen from the results, the incubation time is reduced by the elongation of the wound, although this effect is only significant for large values of θ. This is a consequence of the diffusion term, which aids the accumulation of the EGF at the regions of high curvature. As is to be expected, we observe an exponential increase of the incubation time with θ. The isocurves of the healing time for various wound elongations and θ values are plotted in Figure 8(b). Similarly to the incubation time, the healing time increases with θ and decreases with the wound elongation. However, the increase of the healing time with θ is merely linear, since the EGF accumulation inside the wound reduces the retardation of the healing kinetics.

Finally, we consider the healing of a wound with a more complicated geometry, which initial shape is a four-legged starfish, for various values of θ and β. The initial wound edge is given by the zero level set of the function $\phi = \max(\phi_s, \phi_c)$, where ϕ_s denotes the distance function whose zero level set is the curve

$$x = (a + b\cos\left(2n_{legs}\pi\varphi\right)\cos\left(2\pi s\right),\ y = (a + b\cos\left(2n_{legs}\pi\varphi\right)\sin\left(2\pi s\right)$$

where $\varphi \in [0, 1]$ and n_{legs} denotes the number of legs of the starfish, four in this case, and ϕ_c denotes the distance function whose zero level set is the circle of radius $a - \frac{4}{6}b$ and centered at the origin. By construction, ϕ_s and ϕ_c must be chosen positive at the origin, in order to have ϕ positive inside the wound.

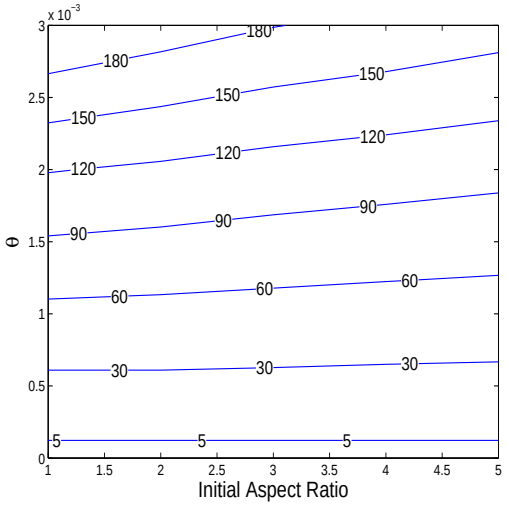

(a) Incubation times (in minutes) for several elliptical wounds and θ values

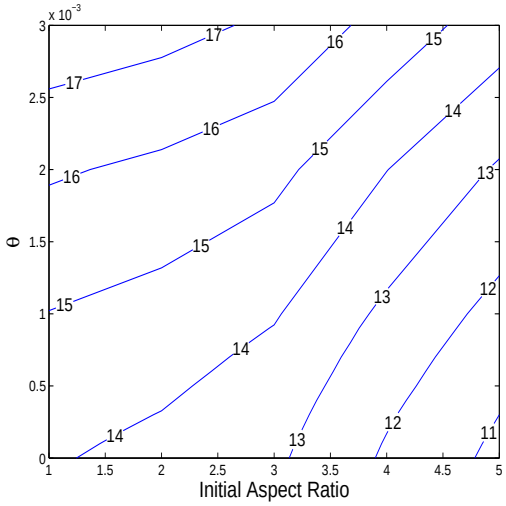

(b) Healing times (in hours) for several elliptical wounds and θ values

Figure 8: Influence on the healing behaviour of the wound morphology and θ. In all the cases, the initial area of the wound is the same.

The initial wound together with the morphology when 30, 60 and 90 % of the initial area is healed are presented in Figure 9. This morphology, although hardly found in practice, illustrates nicely several aspects of the model. First, that the contribution of the curvature to the migration rate may induce a retreat of the wound edge in the concave regions, see Figures 9(d), 9(g), 9(h) and 9(i). Second, that larger values of θ results into longer lag periods for the concave parts of the wound. However, once initiated, the healing of the concave areas is more easily sustained because of soft-impingement effects. And last, that during healing the wound may evolve into several (five in this case) disjoint smaller wounds that heal as isolated islands. We have obtained this behaviour for small values of β or large values of θ, see Figures 9(a), 9(b), 9(c), 9(e), 9(f), 9(h) and 9(i). The irregular shapes at 30% of the wound healed in Figures 9(h) and 9(i) are numerical artifacts due to the size of the time step during incubation periods, 30 seconds, and the complex combination of effects (healing at some parts, growth at others) going on simultaneously at those instants of time.

6 Conclusions

Closure of epidermal wound by cell mitosis and migration is modelled here as a moving interface problem, in which the interface is identified with the advancing front of cells. The level set method is implemented in order to keep track of the wound edge, which allows us to consider complex wound morphologies in a simple manner. The computational method is supplemented with a local grid refinement strategy that enhances the accuracy and efficiency of the complete algorithm.

The physiological analysis carried out in this work enlightens the treatment strategy. It has been proved that unilateral treatmens might lead to unsatisfactory results, since enhancing only the closure rate might lead to longer healing times, whereas enhancing only the diffusion rate might lead to incomplete healing. In addition, taking the closure rate dose-dependent with respect to the EGF concentration results into an effective delay of the healing process, which is more pronounced for high migration rates or large θ values. The morphological analysis of wound healing has shown that healing is much faster for elongated wounds, even without considering any mechanical effects to healing. Furthermore, the undesired retreat of the wound edge at localized areas (the concave

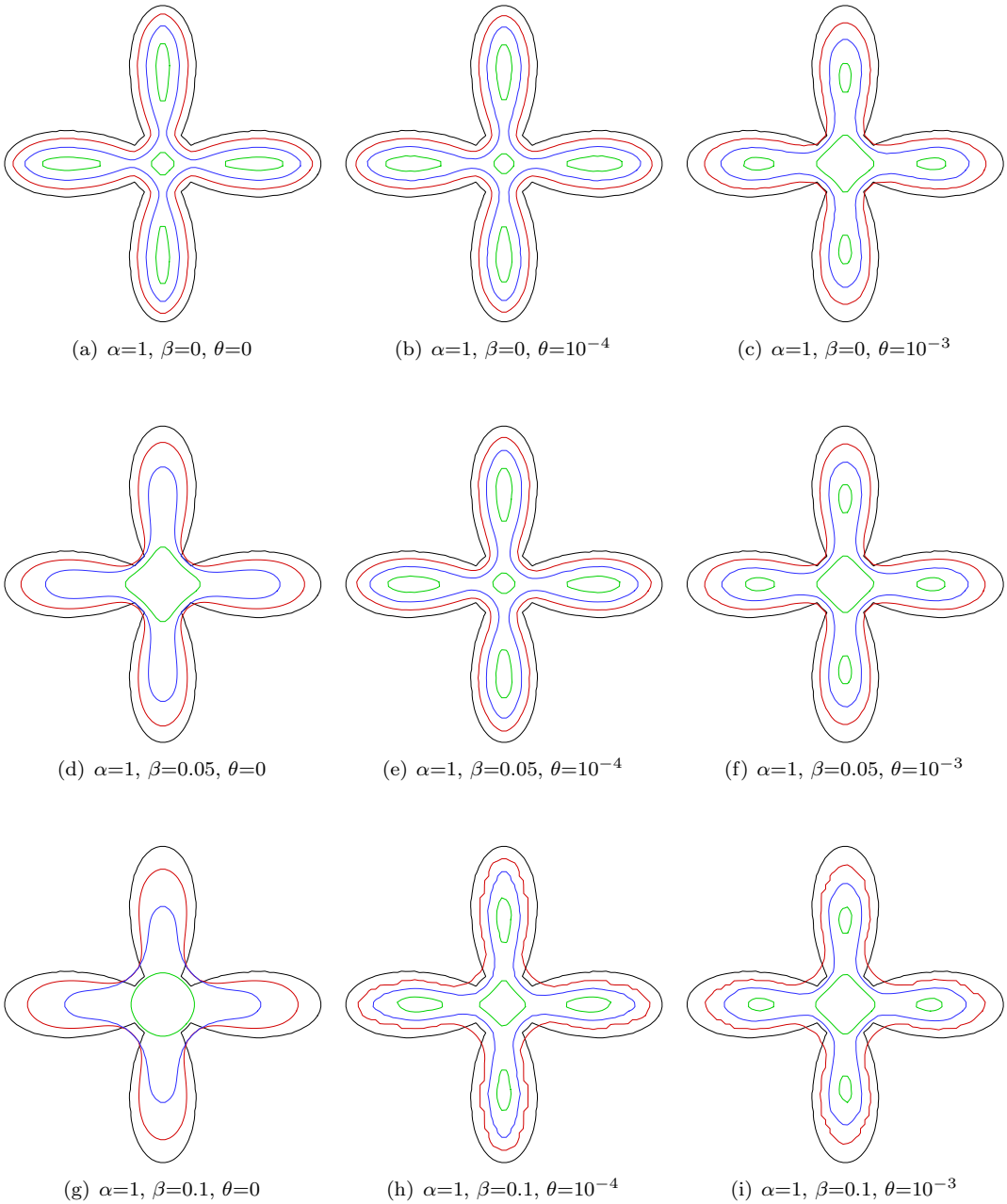

(a) α=1, β=0, θ=0 (b) α=1, β=0, θ=10^{-4} (c) α=1, β=0, θ=10^{-3}

(d) α=1, β=0.05, θ=0 (e) α=1, β=0.05, θ=10^{-4} (f) α=1, β=0.05, θ=10^{-3}

(g) α=1, β=0.1, θ=0 (h) α=1, β=0.1, θ=10^{-4} (i) α=1, β=0.1, θ=10^{-3}

Figure 9: Effect of physiological parameters on the morphology of the wound during healing.

areas of the wound) can be avoided by strict control of the closure rate.

References

[1] D. Adalsteinsson and J. A. Sethian, *A fast level set method for propagating interfaces*, J. Comput. Phys., 118 (1995), pp. 269–277.

[2] J. Adam, *A Simplified Model of Wound Healing (With Particular Reference to the Critical Size Defect)*, Mathematical and Computer Modelling, 30 (1999), pp. 23–32.

[3] J. Arnold and J. Adam, *A Simplified Model of Wound Healing II: The Critical Size Defect in Two Dimensions*, Mathematical and Computer Modelling, 30 (1999), pp. 47–60.

[4] N. F. Britton, *Essential mathematical biology*, Springer Undergraduate Mathematics Series, Springer-Verlag London Ltd., London, 2003.

[5] E. A. Gaffney, K. Pugh, P. K. Maini, and F. Arnold, *Investigating a simple model of cutaneous wound healing angiogenesis*, J. Math. Biol., 45 (2002), pp. 337–374.

[6] S. Maggelakis, *A mathematical model of tissue replacement during epidermal wound healing*, Applied Mathematical Modelling, 27 (2003), pp. 189–196.

[7] S. A. Maggelakis, *Modeling the role of angiogenesis in epidermal wound healing*, Discrete Contin. Dyn. Syst. Ser. B, 4 (2004), pp. 267–273. Mathematical models in cancer (Nashville, TN, 2002).

[8] J. D. Murray, *Mathematical biology. II*, vol. 18 of Interdisciplinary Applied Mathematics, Springer-Verlag, New York, third ed., 2003. Spatial models and biomedical applications.

[9] L. Olsen, J. Sherrat, and P. Maini, *A mechanochemical model for adult dermal wound contraction and the permanence of the contracted tissue displacement profile*, Journal of Theoretical Biology, 177 (1995), pp. 113–128.

[10] S. Osher and R. Fedkiw, *Level Set Methods and Dynamic Implicit Surfaces*, Springer-Verlag, New York, 2003.

[11] S. Osher and J. A. Sethian, *Fronts propagating with curvature-dependent speed: algorithms based on Hamilton-Jacobi formulations*, J. Comput. Phys., 79 (1988), pp. 12–49.

[12] D. Peng, B. Merriman, S. Osher, H. Zhao, and M. Kang, *A PDE-based fast local level set method*, J. Comput. Phys., 155 (1999), pp. 410–438.

[13] J. Sethian, *Level set methods and fast marching methods*, Cambridge University Press, New York, 1999.

[14] J. A. Sethian, *Fast marching methods*, SIAM Rev., 41 (1999), pp. 199–235.

[15] J. Sherratt and J. Murray, *Epidermal wound healing: the clinical implications of a simple mathematical model*, Cell Transplantation, 1 (1992), pp. 365–371.

[16] M. Sussman, P. Smereka, and S. Osher, *A Level Set Approach for Computing Solutions to Incompressible Two-Phase Flow*, J. Comp. Phys., 114 (1994), pp. 146–159.

[17] F. Vermolen, E. van Baaren, and J. Adam, *A simplified model for growth factor induced healing of wounds*, Mathematical and Computer Modelling, 44 (2006), pp. 887–898.

[18] H. Zhao, *A fast sweeping method for Eikonal equations*, Math. Comp., 74 (2005), pp. 603–627.

[19] S. v. d. Zwaag, *Self Healing Materials: An Alternative Approach to 20 Centuries of Materials Science*, Springer Series in Materials Science, Dordrecht, The Netherlands, 2007.

Appendix: Data set of the numerical tests

Of the physiological parameters of the model, only $D = 5 \times 10^{-7}$ cm^2/s [2] and $\lambda = 1.6 \times 10^{-5}1$/s [15] have been estimated. The authors are not aware of valid estimates for the other parameters, and hence these will be treated as fitting parameters in the calculations. In order to simplify the analysis, we fix $P = 5{\cdot}10^{-7}$ $[c]$/s (in which $[c]$ denotes the applied unit of the EGF concentration) and δ=0.1 cm throughout our calculations. The other parameters will be taken depending, on the analysis purposes, as summarized below.

	Figure 4	Figure 5(a)	Figure 5(b)
Geometry (cm)	circular r_0=0.5	circular r_0=0.5	circular r_0=0.5
θ ([c])	$2.5{\cdot}10^{-2}$	$5{\cdot}10^{-4}$ 10^{-3}	$\in [3 \cdot 10^{-5}, 7 \cdot 10^{-3}]$
α (cm/s)	10^{-5}	10^{-5}	10^{-9}, 10^{-7}, $5{\cdot}10^{-7}$ 10^{-6}, $2{\cdot}10^{-6}$, $3{\cdot}10^{-6}$ $4{\cdot}10^{-6}$, $5{\cdot}10^{-6}$, $7{\cdot}10^{-6}$
β (cm^2/s)	$2.1{\cdot}10^{-7}$	$2.1{\cdot}10^{-7}$	0
Ω	[0,1.5]	[0,1.5]	[0,1.5]

Table 2: Physiological parameters for the asymptotic solutions presented in Figures 4 and 5.

	Figure 6	Figure 7	Figure 8	Figure 9
Geometry (cm)	circular r_0=0.5	circular r_0=0.5	elliptical $a=\sqrt{0.25/AR}$ $b=a/AR$ AR=1,. . .,5	starfish a=0.25 b=0.225
θ ([c])	$8{\cdot}10^{-4}$	$\in [0, 10^{-3}]$	$\in [0, 3\cdot 10^{-3}]$	$\in [0, 3\cdot 10^{-3}]$
α (cm/s)	10^{-5}	$\in [10^{-5}, 10^{-4}]$	10^{-5}	1
β (cm^2/s)	$2.1{\cdot}10^{-7}$	0	$2.1{\cdot}10^{-7}$	0, 0.05, 0.1
Ω	[0,1.5]	[0,1.5]	$[0, L_x]\times[0, L_y]$ $L_x = 0.5 + a$ $L_y = 0.5 + b$	[-1,1]x[-1,1]
# internal nodes	499	499	AR, nx, ny 1, 24, 24 2, 29, 20 3, 33, 19 4, 37, 18 5, 39, 17	nx, ny 50, 50
$refnratio$	3	3	3	3
ε (cm)	$1.5{\cdot}10^{-3}$	$1.5{\cdot}10^{-3}$	$\approx 1.33{\cdot}10^{-2}$	$1.31{\cdot}10^{-2}$
Δt_{max} (s)	5	5	30	30
CFL	0.15	0.15	0.15	0.45

Table 3: Physiological and numerical parameters used in the calculation of the results presented in Figures 6-9.